HHS Public Access

Author manuscript

Neurobiol Dis. Author manuscript; available in PMC 2022 November 03.

Published in final edited form as:

Neurobiol Dis. 2022 October 15; 173: 105838. doi:10.1016/j.nbd.2022.105838.

Aberrant brain functional and structural developments in *MECP2* duplication rats

Ming Xu[a,b,1], **Shile Qi**[c,1], **Vince Calhoun**[d], **Jiankun Dai**[e,2], **Bin Yu**[e,3], **Kaiwei Zhang**[e], **Mengchao Pei**[e], **Chenjian Li**[f,g], **Yusheng Wei**[f,g], **Rongtao Jiang**[a], **Dongmei Zhi**[a,b], **Zhimin Huang**[f,g], **Zilong Qiu**[e], **Zhifeng Liang**[e,*], **Jing Sui**[h,*]

[a]Brainnetome Center and National Laboratory of Pattern Recognition, Institute of Automation, Chinese Academy of Sciences, Beijing 100190, China

[b]School of Artificial Intelligence, University of Chinese Academy of Sciences, Beijing, 100190, China

[c]College of Computer Science and Technology, Nanjing University of Aeronautics and Astronautics, Nanjing 211106, China

[d]Tri-institutional Center for Translational Research in Neuroimaging and Data Science (TReNDS), Georgia Institute of Technology, Georgia State University, Emory University, Atlanta, GA 30303, USA

[e]Institute of Neuroscience, Center for Excellence in Brain Science and Intelligence Technology, State Key Laboratory of Neuroscience, CAS Key Laboratory of Primate Neurobiology, Chinese Academy of Sciences, Shanghai 200031, China

[f]Ministry of Education Key Laboratory of Cell Proliferation and Differentiation, Peking University School of Life Sciences, Beijing 100871, China

[g]PKU-IDG/McGovern Institute for Brain Research, Peking-Tsinghua Center for Life Sciences, Beijing 100871, China

[*]Corresponding authors: zliang@ion.ac.cn (Z. Liang), jsui@bnu.edu.cn (J. Sui).
[1]These authors contributed equally to this work.
[2]Present address: Bruker BioSpin PCI; Shanghai, China.
[3]Present address: Department of Neurobiology and Department of Neurology of Second Affiliated Hospital, NHC and CAMS Key Laboratory of Medical Neurobiology, MDP Frontier Science Center for Brain Research and Brain-Machine Integration, Zhejiang University School of Brain Science and Brain Medicine; Hangzhou, 310058, China.

CRediT authorship contribution statement

Ming Xu: Formal analysis, Investigation, Data curation, Writing – original draft, Writing – review & editing, Visualization. **Shile Qi:** Formal analysis, Investigation, Writing – review & editing. **Vince Calhoun:** Writing – review & editing, Funding acquisition. **Jiankun Dai:** Investigation, Funding acquisition. **Bin Yu:** Investigation. **Kaiwei Zhang:** Investigation. **Mengchao Pei:** Investigation. **Chenjian Li:** Investigation. **Yusheng Wei:** Investigation. **Rongtao Jiang:** Writing – review & editing. **Dongmei Zhi:** Writing – review & editing. **Zhimin Huang:** Investigation. **Zilong Qiu:** Writing – review & editing, Funding acquisition. **Zhifeng Liang:** Supervision, Conceptualization, Methodology, Investigation, Resources, Data curation, Writing – review & editing, Project administration, Funding acquisition. **Jing Sui:** Supervision, Conceptualization, Methodology, Resources, Writing – review & editing, Project administration, Funding acquisition.

Declaration of competing interest

The authors report no biomedical financial interests or potential conflicts of interest.

Appendix A. Supplementary data

Supplementary data to this article can be found online at https://doi.org/10.1016/j.nbd.2022.105838.

[h]IDG/McGovern Institute for Brain Research, State Key Laboratory of Cognitive Neuroscience and Learning, Beijing Normal University, Beijing 100875, China

Abstract

Transgenic animal models with homologous etiology provide a promising way to pursue the neurobiological substrates of the behavioral deficits in autism spectrum disorder (ASD). Gain-of-function mutations of *MECP2* cause MECP2 duplication syndrome, a severe neurological disorder with core symptoms of ASD. However, abnormal brain developments underlying the autistic-like behavioral deficits of MECP2 duplication syndrome are rarely investigated. To this end, a human *MECP2* duplication (MECP2-DP) rat model was created by the bacterial artificial chromosome transgenic method. Functional and structural magnetic resonance imaging (MRI) with high-field were performed on 16 male MECP2-DP rats and 15 male wildtype rats at postnatal 28 days, 42 days, and 56 days old. Multimodal fusion analyses guided by locomotor-relevant metrics and social novelty time separately were applied to identify abnormal brain networks associated with diverse behavioral deficits induced by *MECP2* duplication. Aberrant functional developments of a core network primarily composed of the dorsal medial prefrontal cortex (dmPFC) and retrosplenial cortex (RSP) were detected to associate with diverse behavioral phenotypes in MECP2-DP rats. Altered developments of gray matter volume were detected in the hippocampus and thalamus. We conclude that gain-of-function mutations of *MECP2* induce aberrant functional activities in the default-mode-like network and aberrant volumetric changes in the brain, resulting in autistic-like behavioral deficits. Our results gain critical insights into the biomarker of MECP2 duplication syndrome and the neurobiological underpinnings of the behavioral deficits in ASD.

Keywords

MECP2 duplication; Multimodal fusion; Rat brain; Brain development; Autistic spectrum disorder (ASD); Magnetic resonance imaging (MRI)

1. Introduction

Autism spectrum disorder (ASD) is a highly heritable neurodevelopmental disorder characterized by social impairments and inflexible behaviors (Lord et al., 2020), of which treatments are an unmet medical need. One feasible way to pursue the underlying pathophysiology of ASD is to establish transgenic animal models that recapitulate some core autistic behavioral phenotypes (Varghese et al., 2017), assuming such animal models would share some homologous endophenotypes with humans.

Methyl-CpG binding protein 2 (MeCP2) is an essential nuclear protein involved in transcriptional regulation and microRNA processing (Chahrour et al., 2008; Nan et al., 1997; Qiu, 2018). Gain-of-function mutations of the *MECP2* gene lead to MECP2 duplication syndrome, a severe neurological disorder with core symptoms of ASD (Ramocki et al., 2010; Van Esch et al., 2005). Currently, genetically manipulated primate and rodent models with *MECP2* duplication (MECP2-DP) have successfully recapitulated multiple dimensions of autistic symptoms, including abnormal learning abilities, repetitive circular locomotion, and reduced interest in social interactions (Collins et al., 2004; Liu et al., 2016). Recent

studies based on transgenic animal models have demonstrated that overexpression of MeCP2 could cause abnormal dendritic arborization and spine dynamics (Jiang et al., 2013). Excitatory neurotransmission enhancements in the hippocampus and disrupted excitatory-inhibitory balance in neural circuits have also been reported in MECP2-DP mice (Lu et al., 2016; Na et al., 2012). These studies underscore the roles of MeCP2 in brain functional and structural development.

Magnetic resonance imaging (MRI) provides a powerful tool for noninvasively probing macroscale brain functional and structural abnormalities in transgenic animal models. By analyzing brain images, alterations of coordinated functional activity (*i.e.*, functional connectivity) in prefrontal and cingulate networks have been detected in adolescent MECP2-DP monkeys (Cai et al., 2020), and such macroscale dysfunction pattern accounts for not only aberrant behavioral phenotypes in the animal model, but also contributes to human ASD stratification and classification (Cai et al., 2020; Zhan et al., 2020). By examining regional brain functional metrics, a recent imaging study of adult MECP2-DP mice has suggested that focal functional abnormalities involving fALFF (short for *fractional Amplitude of Low-Frequency Fluctuations*) and ReHo (short for *Regional Homogeneity*) alterations especially occur in brain areas relating to emotion and social behaviors (Yu et al., 2020). Notably, MeCP2 expression level varies across brain areas and developmental milestones (Mullaney et al., 2004), and brain development is also intrinsically nonlinear and complex. However, the developmental implications of *MECP2* duplication on brain function and structure, and how the altered brain developments lead to behavioral deficits, are still underexplored. In addition, current imaging studies of animal models primarily focus on a single modality or analyze multimodal imaging data separately. Therefore, the complementary information among different imaging modalities and features (*e.g.*, fALFF and ReHo) is not fully leveraged (Calhoun and Sui, 2016; Sui et al., 2018), highlighting the need for a powerful data-driven tool to mine multimodal complementary information (Calhoun and Sui, 2016; Sui et al., 2020).

To tackle these questions, we established a MECP2-DP rat model manifesting locomotor deficits and reduced social novelty preference. We collected brain functional and structural images of both MECP2-DP rats and wildtype (WT) rats at three developmental milestones, *i.e.*, postnatal 28 days (P28), 42 days (P42), 56 days (P56). Then, we performed multimodal MRI fusion supervised by social novelty time and locomotor-relevant metrics to detect abnormal brain networks underlying various behavioral deficits of MECP2-DP rats. A linear mixed-effect model was established to analyze the developmental implications of atypical *MECP2* levels on brain function and structure spanning the three developmental milestones. Finally, brain networks underlying social deficits and motor deficits were compared to identify the common and unique brain abnormal patterns. We believe our study will gain critical insights into the neurobiological underpinnings of behavioral deficits of MECP2 duplication syndrome and ASD.

2. Materials and methods

2.1. Creation of transgenic MECP2-DP rat model

PAC671D9 (AF031078) DNA was digested with *Not* I. The 99 kb insert which contains all the exons of human *MECP2* was separated from the vector on a pulse-field gel. The fragment was purified on the CL4B column (GE, Cat No: 17015001). The DNA was then washed off the column with microinjection buffer (10 mM Tris pH 8.0; 0.1 mM EDTA) and was injected into rat single-cell zygotes at concentrations of 0.5 ng/ml using standard procedures. Founders and progenies carrying human *MECP2* transgene were identified by PCR from tail DNA and direct sequencing. The full-length human *MECP2* expression was confirmed by Western blot analysis. The transgenic rats were maintained by breeding to wildtype SD rats. All the experiments performed with MECP2-DP rats were controlled by wildtype littermates kept in the same cage.

2.2. Western blot analysis

Rats were anesthetized with pentobarbital sodium (100 mg/kg, MYM Technologies) and rapidly decapitated. The brain was immediately extracted and placed in ice-cold PBS. The prefrontal cortex, hippocampus and cerebellum were dissected and transferred to a 1.5-mL centrifuge tube containing ice-cold RIPA buffer and protease inhibitors (Roche). The tissue was homogenized with an electric homogenizer, then the tube was left on an orbital shaker for 2 h at 4 °C. The cell lysate was centrifuged for 20 min at 12,000 rpm at 4 °C in a microcentrifuge. Supernatants were dissolved in SDS-PAGE sample buffer and boiled for 10 min. Proteins were separated on 8% SDS-PAGE gels. The primary antibodies used were rabbit anti-MeCP2 (1:1000, CST) and mouse anti-β-actin (1:1000, CST). The secondary antibodies used were anti-rabbit and anti-mouse HRP antibodies (1:2000, Sigma-Aldrich). Blots were imaged with a GE Amersham Imager600 system (GE Healthcare, Chicago, IL), and quantified using ImageJ. See Fig. 2A-B in the main text for results.

2.3. Open-field test

The locomotor activity of rats (16 MECP2-DP male rats and 15 WT male rats) was examined using the open-field test at postnatal 63 days old, and each animal was tested only once. After habituation to the environment for 30 min, each rat was placed in the center of an open arena (60 cm × 60 cm × 45 cm). The test animal was allowed to move freely for 30 min and its behavior was tracked by a camera above the arena. General locomotor activity was automatically analyzed by Lab-Stante (AniLab Software and Instruments Co., Ltd., China). See Fig. 3A-C in the main text and Supplementary Table S2 for results.

2.4. Three-chamber test

The sociability of all rats (16 MECP2-DP male rats and 15 WT male rats) was tested in a three-chamber apparatus (90 cm × 45 cm × 45 cm) at postnatal 66 days old, and each animal was tested only once. On the test day, animals were allowed to habituate to the environment for 30 min. A three-step procedure was performed. First, the test animal was placed in the center chamber for the side preference. The time spent on exploring each mesh bucket was 10 min. Second, sociability was tested, in which a male intruder (Animal 1) in one mesh

bucket was introduced to one of the side chambers, while the other bucket was kept empty. The test animal was allowed to explore both chambers for 10 min. Lastly, the social novelty was tested by switching the familiar intruder into the other chamber and introducing a novel male intruder (Animal 2) to the chamber. The test animal was monitored for 10 min as well. The whole process was recorded, and the recorded data were analyzed by Lab-Stante (AniLab Software and Instruments Co., Ltd., China). See Fig. 3D-F in the main text and Supplementary Table S3, S4 for results.

2.5. MRI data collection of rats

Before behavioral tests, both functional MRI and structural MRI were acquired from the 16 male MECP2-DP rats and 15 male WT rats (from six litters) at postnatal 28 days, 42 days, and 56 days, respectively. At each age, 24 or more rats got MRI scans successfully, please see more details in Supplemental Table S1. Rats are weaned at postnatal 28 days old, start adolescence at 42 days old, and start adulthood at 56 days old (Sengupta, 2013). Therefore, brain images collected at the selected developmental milestones would map brain developments across the entire adolescent phase of rats, which largely corresponded to the period of neurodevelopmental disorder (*i.e.*, ASD) with most typical symptoms in humans. Anesthesia was first induced by 3–4% isoflurane, followed by intramuscular administration of dexmedetomidine (0.015 mg/kg). Isoflurane was reduced to 0.2%–0.5% and was combined with continuous subcutaneous infusion of dexmedetomidine (0.03 $mg{\cdot}kg^{-1}{\cdot}hr^{-1}$) for resting-state fMRI (Brynildsen et al., 2017). This anesthesia protocol has proved to only minimally disturb the brain networks and was a viable option for longitudinal imaging studies in rats (Brynildsen et al., 2017; Sumiyoshi et al., 2019). For other scans, dexmedetomidine was stopped, and 2% isoflurane was used. During all imaging sessions, the animal body temperature was maintained at 37 °C ± 0.5 °C by combining a warm water pad and a hot-air blower with temperature feedback (SAII, Stony Brook, NY). The respiratory rate was monitored (Model 1025, SAII, Stony Brook, NY) during imaging and was approximately 80 bpm for resting fMRI and 40 bpm for T2-weighted imaging.

All animal MRI scans were performed on a 9.4 T/30 cm Bruker BioSpec scanner with a rat brain 2 × 2 surface array coil for signal detection. T2-weighted anatomical images were acquired at postnatal 28 days, 42 days and 56 days with the rapid acquisition with refocused echDPs (RARE) sequence, TR 6300 ms, TE 32 ms, RARE factor 8, field of view (FOV) 2.6 cm × 2.3 cm, matrix size 130 × 115, 58 contiguous coronal slices, slice thickness 0.4 mm and 4 averages. The spatial resolution of T2-weighted imaging data was 200 μm × 200 μm × 400 μm. Resting-state fMRI was acquired at postnatal 28 days, 42 days and 56 days using the gradient echo EPI sequence with the following parameters: TR 1 s, TE 15 ms, flip angle 60°, FOV, 2.8 × 2.5 cm, matrix size 83 × 74, slice number 29, and slice thickness 0.6 mm. Six hundred EPI volumes were acquired for each run, and two runs were obtained for each session. The acquisition resolution of the rest fMRI was 337 μm × 337 μm × 600 μm.

2.6. Rat MRI data preprocessing

The T2-weighted anatomical images of normal animals were firstly skull stripped using a semi-automated brain extraction method developed by Delora et al. (2016) and followed by correction of signal intensity non-uniformity resulted from surface coil reception

using the *N4BiasFieldCorrection* function of Advanced Normalization Tools (ANTs, http://picsl.upenn.edu/software/ants/). All corrected data were then resampled to an isotropic voxel size of 200 μm × 200 μm × 200 μm. The preprocessed images from each individual animal were segmented into three tissue classes (gray matter, GM; white matter, WM; cerebrospinal fluid, CSF) without *a priori* probability maps using the *atropos* function of ANTs. For each age group, the WM probability map from one representative animal was selected as the initial template. The WM probability maps from all other animals in the same age group were spatially normalized to the space of the selected representative animal using an initial affine registration step and a subsequent diffeomorphic transformation step (*i.e.*, non-linear warping). All co-registered individual WM probability maps of each age group were then averaged separately. Then, the averaged WM probability maps of each two adjacent age groups were normalized to the space of the older group (*i.e.*, P28 to P42, and P42 to P56). By concatenating the transformation information from each registration step, the GM, WM and CSF of each animal from P28 and P42 were directly normalized to the space of the P56 average brain. We employed this warp strategy for large structural differences between P56 and younger brains. This registration strategy has been shown to yield a higher level of accuracy (Baloch et al., 2009). All the registration results were visually inspected by using well-defined structures (*e.g.*, ventricles, anterior commissure, internal capsule, corpus callosum, brain boundaries, *etc.*) as references. Finally, all the co-registered datasets from different ages were averaged separately to obtain space-normalized and age-specific GM/WM/CSF probability maps.

After the construction of GM/WM/CSF probability maps, voxel-based morphometry (VBM) analysis was carried out using the Statistical Parametric Mapping 8 (SPM8; Wellcome Trust Centre for Neuroimaging, London, 222 UK) toolbox. First, all original T2-weighted anatomical images, as well as the space-normalized and age-specific prior tissue probability maps, were resized by a factor of 10 according to the work of Sumiyoshi et al. (2014). Then, each image was segmented into probability maps of GM, WM and CSF using the unified segmentation approach, which enables image registration, tissue classification, and bias correction to be combined within the unified generation model (Ashburner and Friston, 2005). For the unified segmentation steps, the default settings in the SPM8 toolbox were used except that the human tissue priors were replaced with age-specific tissue priors constructed in this study. Afterward, the results were further processed using the *DARTEL* implemented in SPM8 to produce a more accurate registration of segmented tissue maps. For this step, the default settings were used. Then, the normalized tissue class maps of each animal were modulated and smoothed with a 6 mm full width at half maximum (FWHM) Gaussian kernel (for the resized images), resulting in a volumetric map of gray matter (GMV), white matter (WMV) and cerebrospinal fluid.

The average of aligned functional volumes was rigidly co-registered to its T2-weighted anatomical image. All anatomical images were skull stripped using a semi-automatic method developed by Delora et al. (2016) and were subsequently warped to the space of a parcellated MRI rat brain atlas with the following steps: For each age group, the anatomical image from one representative animal was selected as an initial template. The anatomical images from all other animals in the same age group were first linearly and subsequently non-linearly normalized to the space of the selected representative animal. The

normalized anatomical images of each age group were then averaged separately. Afterward, the averaged image of P28 and P42 was co-registered to that of P42 and P56, respectively. Further, the average anatomical image of P56 was normalized to the parcellated rat brain atlas. Finally, all the functional images of each animal were directly warped to the space of the parcellated atlas by concatenating the transformation from each registration step. All the registration processes were carried out by ANTs. After registration, all functional images were pre-processed with steps for motion, white matter, and cerebrospinal fluid signal regression, de-trending, 0.01–0.1 Hz band-pass filtering and smoothing with a 0.6 mm FWHM Gaussian kernel. The pre-processed data without band-pass filtering and smoothing were used to generate ReHo map by calculating Kendall's coefficient of concordance of the time series of a given voxel with those of its nearest neighbors (26 voxels). The pre-processed data with band-pass filtering and smoothing were used to generate fALFF (0.01 Hz–0.08 Hz) maps. Both ReHo and fALFF calculations were carried out using the free software REST (Resting-State fMRI Data Analysis Toolkit V1.8, http://restfmri.net/forum/REST_V1.8). All the ReHo and fALFF maps were smoothed with a 0.4-mm FWHM Gaussian kernel.

2.7. Multimodal fusion with reference

As shown in Fig. 1, we performed systematic, data-driven analyses, aiming to map reliable multimodal MRI signatures of brain networks associated with multiple behavioral deficits in MECP2-DP rats.

After preprocessing, we got three $N_X^i \times N_Y^i \times N_Z^i$ feature matrices ($i = 1, 2, 3$ referred to fALFF, ReHo and GMV respectively; N_X, N_Y, N_Z referred to dimensions of feature matrices) for each rat, then each three-dimensional feature matrix was reshaped into a one-dimensional feature vector. The feature vectors of all rats at different developmental stages were stacked, resulting in the following longitudinal feature matrices:

$$X^i = \begin{pmatrix} X_{P28}^i \\ X_{P42}^i \\ X_{P56}^i \end{pmatrix}_{\left(N_{sub}^{P28} + N_{sub}^{P42} + N_{sub}^{P56}\right) \times N_{voxel}^i} \quad i = 1, 2, 3; \tag{1}$$

Each block of X^i was a subject-by-voxel feature matrix $\left(1 \times N_{voxel}^i\right)$ at a specific time point (*i.e.*, postnatal 28 days, 42 days, and 56 days). The fusion with reference method — "MCCAR+jICA" (multimodal canonical correlation analysis with reference plus joint independent component analysis) (Qi et al., 2018) was adopted to identify the multimodal brain networks associated with a behavioral reference (Fig. 1A). The behavioral reference was a $\left(N_{sub}^{P28} + N_{sub}^{P42} + N_{sub}^{P56}\right) \times 1$ numerical vector. As the behavior test was only conducted once after maturing, the references for a rat at different developmental stages were the same. After fusion, each longitudinal feature matrix X^i could be decomposed as K modality-specific independent components (ICs) S^i and corresponding loading matrix A^i under the supervision of behavioral references, thus $X^i = A^i \times S^i$. In this study, the component number K was estimated to be 11 based on a modified minimum description length criterion (Li

et al., 2007). Intuitively, the IC marks regions involved in a network or the contributions of voxels to the corresponding group-level loadings (in the following of text, *independent components*, *brain covarying patterns*, and *brain networks* are interchangeable terms), and the elements of the loading matrix represent how identified independent components make up the feature matrix of a specific subject, or the contribution of each independent component to the subject-wise feature matrix.

Further, the loading matrix A^i was partitioned into 3 blocks:

$$A^i = \begin{pmatrix} A^i_{P28} \\ A^i_{P42} \\ A^i_{P56} \end{pmatrix} \tag{2}$$

Each block was a subject-by-K (number of components) matrix and was regarded as the loading matrix for a specific time point (*i.e.*, postnatal 28, 42, and 56 days), for example, $X^i_{P28} = A^i_{P28} \times S^i$. By analyzing the longitudinal loading matrix (see Fig.S1), one or more components with behavior-related and group-discriminative loadings were identified as significant brain networks underlying the behavioral phenotypes and were presented in *Results* (Fig. 4A and Fig. 5A).

Finally, we compared the brain network underlying different behavioral phenotypes (*i.e.*, social novelty time and motor ability), and the common and unique brain abnormalities in different behavioral domains were identified.

2.8. Statistical analysis

A two-tailed t-test was used for comparisons of behavioral metrics between MECP2-DP rats and WT rats. A linear mixed-effect model (LME) was established to delineate the developmental trajectory of each brain network based on the corresponding longitudinal loadings (Fig. 1B). Only rats that completed imaging collections at three time points were included in the longitudinal analysis (MECP2-DP = 9, WT = 12). For rat i with genotype k at time point j, the loading coefficient a_{ikj} was modeled as Eq. (3).

$$\begin{aligned} a_{ikj} = \alpha + \mu_i + \beta_k gene_{ik} + \tau_j time_{ij} \\ + \lambda_{kj} gene_{ik} : time_{ij} + \varepsilon_{ikj} \end{aligned} \tag{3}$$

ANOVA (Analysis of variance) was used to test the main effects of genotype and time, and the interaction effect of genotype-by-time. Therefore, the question regarding the impact of genotype on brain network developments transformed to a statistical problem regarding the main effect of genotype (gross impacts of genotype on brain developments) and the interaction effect of genotype-by-time (impacts of genotype on brain developmental trajectories during the given age range).

To evaluate the behavioral correlation of each IC, the Pearson correlation coefficient was calculated between corresponding loadings of the IC at postnatal 56 days old and the behavioral metrics collected after maturing (around postnatal 60 days old) (Fig. 1C).

Multiple Comparisons were controlled using the false discovery rate (FDR, Benjamini-Hochberg method), and all FDR corrected p values were star marked in figures. All analyses were performed in MATLAB R2016b (MathWorks, https://www.mathworks.com/).

2.9. Ethical approval

All experimental procedures for nonhuman primate research in this study were approved by the Institutional Animal Care and Use Committee at the Institute of Neuroscience and the Biomedical Research Ethics Committee, Shanghai Institutes for Biological Sciences, Chinese Academy of Sciences, and conformed to the National Institutes of Health guidelines for the humane care and use of laboratory animals. All applicable institutional and/or national guidelines for the care and use of animals were followed.

3. Results

3.1. Increased MeCP2 expression in the brain of MECP2-DP rats

Western blot analysis showed a global increase in MeCP2 protein across the rat brain, especially in the cerebral cortex and hippocampus, with almost doubled expression compared to WT rats (Fig. 2A-B). These results confirm that genetically manipulated rats are a viable model to study the consequences of MeCP2 overexpression. In addition, MECP2-DP showed a slower body weight increase (Fig. 2C) and a lower survival rate (Fig. 2D).

3.2. Behavioral deficits in MECP2-DP rats

Compared with wildtype rats, MECP2-DP rats manifested significantly less locomotor duration ($p = 0.0156$, $t_{29} = -2.57$), distance ($p = 0.0003$, $t_{29} = -4.07$) and lower speed ($p = 0.0124$, $t_{29} = -2.67$) in the open-field test (Fig. 3A-C). More importantly, in the three-chamber test, MECP2-DP rats exhibited a decreased preference ($p = 0.0030$, $t_{29} = -3.23$) for interacting with novel animals (Fig. 3D-F). Such behavioral deficits in social novelty can be considered as one of the core phenotypes of ASD (Silverman et al., 2010).

3.3. Aberrant developments of brain network underlying social deficits in MECP2-DP rats

Under the guidance of social novelty time, developmental trajectories of three brain networks were identified to be significantly different between the MECP2-DP and WT rats (Fig. 4), while other components showed no between-group differences nor behavioral associations. The multimodal brain networks underlying social deficits are shown in Fig. 4A, where the red/blue areas represent positive/negative Z-scored spatial map. Gain-of-function mutations of *MECP2* significantly reduced the ReHo in the dorsal medial prefrontal cortex (dmPFC) and retrosplenial cortex (RSP), and increased the ReHo ($p_{gene} = 0.0035$, $F_{1,57} = 9.28$, FDR corrected $p < 0.05$) in the left primary somatosensory cortex (S1). fALFF of a network composed of dmPFC, RSP, visual cortex (V1/V2) and right motor cortex (M1/M2) was significantly decreased in MECP2-DP rats compared with WT rats ($p_{gene} =$

0.0099, $F_{1,57} = 7.12$). Meanwhile, the GMV of the hippocampus was significantly increased ($p_{gene} = 0.0037$, $F_{1,57} = 9.17$, FDR corrected $p < 0.05$) in MECP2-DP rats. Notably, the identified functional-structural network did not exhibit significant changes along the three developmental milestones ($p_{time} > 0.05$ and $p_{interaction} > 0.05$ for all modalities).

Both the fALFF ($r = -0.4257$, $p = 0.0213$) and the ReHo ($r = -0.3768$, $p = 0.0439$) components showed negative correlations with social novelty time. Namely, the more severe novelty preference reduction in rats, the lower fALFF and ReHo of the network encompassing dmPFC and RSP (Fig. 4C). Meanwhile, the GMV component also showed a negative trend, however, the p-value did not reach significance ($r = -0.2643$, $p > 0.05$).

3.4. Aberrant developments of brain network underlying motor ability in MECP2-DP rats

The first principal component of three locomotor metrics (distance, speed, and duration) was regarded as a metric to depict the motor ability of rats (see Fig.S2). Under the guidance of the motor ability metrics, developmental trajectories of three brain networks were identified to be prominently altered between MECP2-DP rats and wildtype rats (Fig. 5), while other components showed no between-group differences nor behavioral associations. The multimodal brain network underlying motor deficits is shown in Fig. 5A. fALFF of a network composed of the medial orbital cortex, dmPFC, M1/M2, RSP, pineal gland and pontine nuclei was decreased in MECP2-DP rats compared with wildtype rats ($F_{1,57} = 5.5302$, $p_{gene} = 0.0222$). The ReHo reductions were found in a network primarily composed of the right motor cortex, right somatosensory cortex, RSP, visual cortex of MECP2-DP rats ($F_{1,57} = 9.8067$, $p_{gene} = 0.0027$, FDR corrected $p < 0.05$). Both fALFF ($F_{2,57} = 10.8699$, $p_{time} = 0.0001$, FDR corrected $p < 0.05$) and ReHo in the identified network ($F_{2,57} = 10.7651$, $p_{time} = 0.0001$, FDR corrected $p < 0.05$) increased along the three developmental milestones of both MECP2-DP rats and wildtype rats. GMV of the thalamus was identified to be reduced in MECP2-DP rats ($F_{1,57} = 7.4968$, $p_{gene} = 0.0082$), whereas no significant changes of GMV in the thalamus were found along the three developmental milestones ($p_{time} > 0.05$). Notably, no significant impacts of gain-of-function mutations of *MECP2* on the developmental trajectories of the identified multimodal brain network were found during the given age range ($p_{interaction} > 0.05$ for all components, see Fig. 5B).

Regarding the behavioral associations (Fig. 5C), all identified networks showed significantly negative correlations with motor ability. Namely, the more severe motor deficits, the more fALFF and ReHo reductions in the motor cortex, dmPFC, RSP and visual cortex, and the more GMV reductions in the thalamus.

3.5. Converged functional alterations underlying behavioral deficits in MECP2-DP rats

The multimodal networks underlying social deficits and motor deficits overlapped in some brain regions. As shown in Fig. 6A, networks associated with social deficits and motor deficits were marked in blue and red respectively, and the brightness of color showed the absolute value of Z-scored spatial map. Regions of dmPFC and RSP were both involved in the fALFF networks underlying social deficits and motor deficits, whereas the fALFF network associated with motor deficits additionally encompassed more regions of the motor cortex and medial orbital cortex. The ReHo network underlying social deficits involved

more regions of the dmPFC, and the ReHo network underlying motor deficits involved more regions of M1/M2. The two ReHo networks both included regions of RSP. Regarding the volumetric changes of gray matter, few regions were overlapped.

Correlation analysis (Fig. 6B-C) showed that the fALFF ($r = -0.4845$, $p = 0.0077$) and ReHo ($r = -0.3871$, $p = 0.0380$) networks underlying social deficits negatively correlated with motor ability scores, and the fALFF network ($r = -0.3684$, $p = 0.0492$) underlying motor deficits negatively correlated with social novelty time. Considering the large, overlapped regions between the fALFF networks underlying motor deficits and social deficits, these results suggest that the neurobiological bases of abnormal behavioral phenotypes induced by *MECP2* duplication converge onto the fALFF decrease of a core network primarily composed of dmPFC and RSP.

4. Discussion

This study illustrated the developmental implications of *MECP2* duplication on brain function and structure underlying behavioral deficits *via* a data-driven multimodal fusion. We discovered altered developments of multimodal brain networks associated with the social ability and motor ability in MECP2-DP rats (Fig. 4 and Fig. 5), primarily involving reduced functional activity and reduced regional homogeneity in the dmPFC, RSP and motor cortex, and overgrowth of the hippocampus, and reduced gray matter volume of the thalamus. By comparing networks underlying social deficits and motor deficits (Fig. 6), we further suggest aberrant functional developments of a core network composed of dmPFC and RSP underlie various behavioral phenotypes induced by *MECP2* duplication.

4.1. Multimodal network underlying social deficits of MECP2-DP rats

A function-structure joint component mainly composed of the dmPFC, RSP and hippocampus was identified to be significantly associated with social deficits in MECP2-DP rats (Fig. 4). dmPFC and RSP are two critical components of the default-mode-like network in rats (Gozzi and Schwarz, 2016; Lu et al., 2012), and are comparable to the anterior-posterior default mode network in humans. Anatomically, dmPFC and RSP interconnect to numerous regions involved in social information processing (Apps et al., 2016; Vann et al., 2009), which presents some evidence to support our results. A recent study based on *Shank3* mutant mice has demonstrated the crucial linkage between pyramidal cell hypoactivity of the dmPFC and social dysfunctions (Guo et al., 2019). Another study has reported that the disrupted activities of layer V neurons in RSP are associated with pharmacologically induced dissociation states and social interaction deficits in mice (Vesuna et al., 2020), suggesting the involvement of RSP in social behavior regulations. Moreover, imaging studies of other rodent models with ASD-relevant genetic mutations also support the roles of dmPFC and RSP dysfunction in social deficits (Liska et al., 2018; Pagani et al., 2019). These studies are consistent with our results and support the associations between the identified brain dysfunction patterns and social deficits in MECP2-DP rats.

Additionally, the social-deficit-related dysfunctional network also indicates increased ReHo in the left S1. S1 processes afferent somatosensory input and contributes to sensory and motor information integration (Borich et al., 2015). Abnormal sensory processing has been

increasingly noticed in ASD (Kern et al., 2006; Liss et al., 2006), and the associations between abnormal sensory function and social deficits in ASD have also been reported (Tavassoli et al., 2018). Indeed, social behavior, which is typically damaged in ASD, is complex and depends on detecting and integrating multiple sensory modalities (Chen and Hong, 2018). Therefore, abnormalities of S1 possibly contribute to social deficits *via* disturbing information integration.

Hippocampal overgrowth was also prominent in the identified network. One study of the valproate rat model of ASD has underscored the mediation function of GABA on hippocampal volume (Cloarec et al., 2019), and another study have demonstrated the great influence of *MECP2* dysfunction on GABAergic neurons (Chao et al., 2010). Additionally, atypical MeCP2 levels also alter synaptogenesis and the dendritic complexity of the hippocampus (Chao et al., 2007). These studies suggest a possible implication of atypical *MECP2* levels on hippocampal volume development. Furthermore, experiments *in vitro* have shown that the hippocampus sends monosynaptic excitatory glutamatergic projections to the mPFC (Kamiyama et al., 2011) and interconnects to the RSP *via* the cingulate tract (Hsu et al., 2016). Such an mPFC-hippocampus-RSP anatomical pathway suggests a potential linkage between focal functional abnormalities in dmPFC/RSP and hippocampal structural changes, which are in accordance with our identified multimodal brain networks.

4.2. Multimodal network underlying motor deficits

A multimodal brain network associated with motor deficits of MECP2-DP rats was also identified. Reduced ReHo was observed in regions of the motor cortex, right S1, and visual cortex. The motor cortex encodes the motor-related neural signals *via* coordinated activities among particular neural populations (Jackson et al., 2003; Torre et al., 2016). Emerging evidence based on rat models of Rett syndrome has shown that MeCP2 disruption induced imbalanced inhibition of the motor cortex (Li et al., 2021), suggesting the role of MeCP2 level on coordinated functional activities in the motor cortex. Furthermore, S1 has rich fiber pathways interconnected with the motor cortex, and interactions between the S1 and motor cortex underpin accurate movement control (Borich et al., 2015; Perruchoud et al., 2014). These studies are in accordance with our results and suggest that altered functional activities in the motor cortex and S1 contribute to the motor dysfunction induced by *MECP2* duplication.

Volumetric reduction of the thalamus was observed in the motor-related network. The rat thalamus processes and relays sensory information to the cortex, and regulates the voluntary motor function through basal ganglia circuitry (Smith et al., 2004), supporting the role of thalamic maldevelopments in motor deficits. MeCP2 is also an essential regulator for the normal development of the thalamus (Blue et al., 2011; Zhang et al., 2010), suggesting the impacts of atypical *MECP2* levels on the volume of the thalamus.

Interestingly, focal functional abnormalities in dmPFC and RSP also presented in the motor-related network. Indeed, both RSP and dmPFC play important roles in motor function in addition to social ability. Anatomically, RSP integrates information from the hippocampal formation and various sensory and motor cortices, and RSP also involves in path integration and navigation (Vann et al., 2009). dmPFC also has rich connections with the motor and

somatosensory cortex and is pivotal for temporal and flexible control of behaviors (Barthas and Kwan, 2017; Narayanan and Laubach, 2006). Therefore, effective collaborations of dmPFC and RSP underlie a broad range of normal behaviors, which also lead them to be more vulnerable in MECP2-DP rats.

4.3. The impact of MECP2 duplication on the developmental trajectory

Longitudinally, our study indicates the impacts of *MECP2* duplication on the brain developmental trajectory are not significant during adolescence of rats (the interaction effect of genotype-by-time is not significant, see Fig. 4B and Fig. 5B). The rat brain undergoes a rapid maturational process by postnatal 15 days old, and reaches the peak in synaptic density and myelination at around postnatal 20–21 days old (approximately equivalent to 2–3 years old of human) (Bockhorst et al., 2008; Micheva and Beaulieu, 1996). During the postnatal 28 to 56 days old, the rat brain reaches a plateau of gray matter volume and synapse density, experiencing ongoing myelination and refinement of cognitive-dependent circuitry (Semple et al., 2013). Additionally, studies have suggested that brain anatomical and functional differences in ASD manifest before the core autistic symptoms emerge at approximately age 2 years in humans (Emerson et al., 2017; Hazlett et al., 2017). However, the earliest imaging time point of the MECP2-DP rat is postnatal 28 days old (approximately equivalent to age 7–8 years in humans) (Semple et al., 2013). Therefore, the current study may already pass the stage when brain functional and structural changes induced by *MECP2* duplication first emerge.

4.4. Implications for human ASD studies

Anterior-posterior default mode network (DMN) dysfunction is widely reported in human ASD patients. Imaging studies have demonstrated that task-related suppression of the DMN is disturbed in human ASD (Kennedy and Courchesne, 2008; Kennedy et al., 2006), and the global and local organizations of DMN are also disrupted in ASD and are associated with social impairments (Padmanabhan et al., 2017; Rane et al., 2015). The medial prefrontal cortex and post cingulate cortex, which are two key nodes of the anterior and posterior DMN respectively, have also demonstrated reduced activations in self-referential processing tasks and theory-of-mind tasks in human ASD (Kana et al., 2015; Lombardo et al., 2009; Morita et al., 2012), further supporting the pivotal roles of the two DMN nodes in social deficits in human ASD. These results are largely in accordance with our observations of anterior-posterior default-mode-like network abnormalities in MECP2-DP rats, suggesting a possible evolutionarily conserved linkage of DMN dysfunction and social deficits.

4.5. Limitations and future directions

For multimodal fusion analysis of longitudinal images, the lack of longitudinal behavioral metrics (*i.e.*, social novelty time, locomotor speed, and locomotor distance) possibly limits the power of identifying age-dependent brain alteration patterns. However, the timing of behavioral experiments in the present study was determined by several practical and scientific reasons. First, rat behavioral phenotyping is generally conducted in adulthood. Behavioral phenotyping (*i.e.*, the open-field test and social novelty test) for those juvenile rats is difficult experimentally, especially at postnatal 28 days old. It has also been shown that young- and middle-aged rodents exhibit different behavioral patterns (Eltokhi et al.,

2020; Shoji and Miyakawa, 2019), making it hard to compare behavioral metrics across different developmental stages. Behavioral tests that recapitulate neuropsychiatric symptoms for a wide age range of rodents are still underexplored. Moreover, the present study may not fully detect the impacts of *MECP2* duplication on brain developmental trajectories, suggesting further imaging studies of MECP2-DP animal models at an earlier developmental milestone and with longer follow-up observations. The present study utilized an anesthetic protocol that combines low dose dexmedetomidine and isoflurane. This anesthetic regimen can maintain stable sedation for over 4 h with successful fMRI experiments and does not affect the fMRI response separated by 1 week (Lu et al., 2012; Sumiyoshi et al., 2019), suggesting its feasibility and safety in longitudinal fMRI studies. We have also established a control group to ensure that anesthesia did not bias our results. However, none of the anesthetic protocols is ideal for all experimental conditions, more effort is needed to develop anesthetic protocols that minimally affect neuronal activity and minimally interfere with neurovascular coupling.

In conclusion, by performing behavior-guided fusion analyses in rats, we fully leveraged the information from multimodal and longitudinal imaging data, providing a unique view for studying the relationship between brain development and behavioral deficits induced by *MECP2* duplication. Functional alterations in the default-mode-like network were identified to be closely linked with social and motor impairments in MECP2-DP rats. Overall, our work gives critical insights into the biomarker of MECP2 duplication syndrome and the neurobiological underpinnings of the behavioral deficits in ASD, highlighting the power of multimodal fusion analysis.

Supplementary Material

Refer to Web version on PubMed Central for supplementary material.

Acknowledgments

Jing Sui and Zhifeng Liang designed the study; Ming Xu and Shile Qi contributed to the data analysis; Ming Xu and Jing Sui wrote the manuscript; Jiankun Dai, Bin Yu, Kaiwei Zhang, Mengchao Pei, Chenjian Li, Yusheng Wei, Zhimin Huang contributed to the animal model, multimodal imaging and behavioral data; Zhifeng Liang, Zilong Qiu, Shile Qi and Vince Calhoun revised the paper. All authors contributed on result interpretation and discussion.

Funding

This work is supported in part by the Natural Science Foundation of China (No. 82022035, 61773380, 31625013, 81941015, 82021001 and 81801354), the Strategic Priority Research Program of the Chinese Academy of Sciences (XDBS01060200), the National Institute of Health (1R01MH117107, R01EB020407, 1R01MH094524), and the National Science Foundation (2112455). Program of Shanghai Academic Research Leader, the Open Large Infrastructure Research of Chinese Academy of Sciences, the Shanghai Municipal Science and Technology Major Project (No. 2018SHZDZX05), Guangdong Key Scientific and Technological Project (No. 2018B030335001).

Data availability

Data will be made available on request.

References

Apps MAJ, et al. , 2016. The anterior cingulate gyrus and social cognition: tracking the motivation of others. Neuron 90, 692–707. [PubMed: 27196973]

Ashburner J, Friston KJ, 2005. Unified segmentation. Neuroimage 26, 839–851. [PubMed: 15955494]

Baloch S, et al. , 2009. Quantification of brain maturation and growth patterns in C57BL/6J mice via computational neuroanatomy of diffusion tensor images. Cereb. Cortex 19, 675–687. [PubMed: 18653668]

Barthas F, Kwan AC, 2017. Secondary motor cortex: where 'Sensory' Meets 'Motor' in the rodent frontal cortex. Trends Neurosci 40, 181–193. [PubMed: 28012708]

Blue ME, et al., 2011. Temporal and Regional Alterations in NMDA Receptor Expression in Mecp2-Null Mice, 294, pp. 1624–1634.

Bockhorst KH, et al. , 2008. Early postnatal development of rat brain: in vivo diffusion tensor imaging. J. Neurosci. Res 86, 1520–1528. [PubMed: 18189320]

Borich MR, et al. , 2015. Understanding the role of the primary somatosensory cortex: opportunities for rehabilitation. Neuropsychologia 79, 246–255. [PubMed: 26164474]

Brynildsen JK, et al. , 2017. Physiological characterization of a robust survival rodent fMRI method. Magn. Reson. Imaging 35, 54–60. [PubMed: 27580522]

Cai DC, et al. , 2020. MECP2 duplication causes aberrant GABA pathways, circuits and behaviors in transgenic monkeys: neural mappings to patients with autism. J. Neurosci 40, 3799–3814. [PubMed: 32269107]

Calhoun VD, Sui J, 2016. Multimodal fusion of brain imaging data: a key to finding the missing link(s) in complex mental illness. Biol. Psychiatry Cognit. Neurosci. Neuroimag 1, 230–244.

Chahrour M, et al. , 2008. MeCP2, a key contributor to neurological disease, activates and represses transcription. Science 320, 1224–1229. [PubMed: 18511691]

Chao H-T, et al. , 2007. MeCP2 controls excitatory synaptic strength by regulating glutamatergic synapse number. Neuron 56, 58–65. [PubMed: 17920015]

Chao H-T, et al. , 2010. Dysfunction in GABA signalling mediates autism-like stereotypies and Rett syndrome phenotypes. Nature 468, 263–269. [PubMed: 21068835]

Chen P, Hong W, 2018. Neural circuit mechanisms of social behavior. Neuron 98, 16–30. [PubMed: 29621486]

Cloarec R, et al. , 2019. Pyramidal neuron growth and increased hippocampal volume during labor and birth in autism. Science. Advances 5, eaav0394. [PubMed: 30746473]

Collins AL, et al. , 2004. Mild overexpression of MeCP2 causes a progressive neurological disorder in mice. Hum. Mol. Genet 13, 2679–2689. [PubMed: 15351775]

Delora A, et al. , 2016. A simple rapid process for semi-automated brain extraction from magnetic resonance images of the whole mouse head. J. Neurosci. Methods 257, 185–193. [PubMed: 26455644]

Eltokhi A, et al. , 2020. Behavioral tests assessing neuropsychiatric phenotypes in adolescent mice reveal strain- and sex-specific effects. Sci. Rep 10, 11263. [PubMed: 32647155]

Emerson RW, et al. , 2017. Functional neuroimaging of high-risk 6-month-old infants predicts a diagnosis of autism at 24 months of age. Sci. Transl. Med 9.

Gozzi A, Schwarz AJ, 2016. Large-scale functional connectivity networks in the rodent brain. NeuroImage 127, 496–509. [PubMed: 26706448]

Guo B, et al. , 2019. Anterior cingulate cortex dysfunction underlies social deficits in Shank3 mutant mice. Nat. Neurosci 22, 1223–1234. [PubMed: 31332372]

Hazlett HC, et al. , 2017. Early brain development in infants at high risk for autism spectrum disorder. Nature 542, 348–351. [PubMed: 28202961]

Hsu L-M, et al. , 2016. Constituents and functional implications of the rat default mode network. Proc. Natl. Acad. Sci 113, E4541–E4547. [PubMed: 27439860]

Jackson A, et al., 2003. Synchrony between neurons with similar muscle fields in monkey motor cortex, 38, pp. 115–125.

Jiang M, et al. , 2013. Dendritic arborization and spine dynamics are abnormal in the mouse model of MECP2 duplication syndrome. J. Neurosci 33, 19518–19533. [PubMed: 24336718]

Kamiyama H, et al. , 2011. Mechanisms underlying ketamine-induced synaptic depression in rat hippocampus-medial prefrontal cortex pathway. Neuroscience 177, 159–169. [PubMed: 21163337]

Kana RK, et al. , 2015. Aberrant functioning of the theory-of-mind network in children and adolescents with autism. Mol. Autism 6, 59. [PubMed: 26512314]

Kennedy DP, Courchesne E, 2008. The intrinsic functional organization of the brain is altered in autism. Neuroimage 39, 1877–1885. [PubMed: 18083565]

Kennedy DP, Redcay E, Courchesne E, 2006. Failing to deactivate: resting functional abnormalities in autism. Proc. Natl. Acad. Sci. U. S. A 103, 8275–8280. [PubMed: 16702548]

Kern JK, et al. , 2006. The pattern of sensory processing abnormalities in autism. Autism 10, 480–494. [PubMed: 16940314]

Li YO, et al. , 2007. Estimating the number of independent components for functional magnetic resonance imaging data. Hum. Brain Mapp 28, 1251–1266. [PubMed: 17274023]

Li J, et al. , 2021. Collapse of complexity of brain and body activity due to excessive inhibition and MeCP2 disruption. Proc. Natl. Acad. Sci. U. S. A 118.

Liska A, et al. , 2018. Homozygous loss of autism-risk gene CNTNAP2 results in reduced local and long-range prefrontal functional connectivity. Cereb. Cortex 28, 1141–1153. [PubMed: 28184409]

Liss M, et al. , 2006. Sensory and attention abnormalities in autistic spectrum disorders. Autism 10, 155–172. [PubMed: 16613865]

Liu Z, et al. , 2016. Autism-like behaviours and germline transmission in transgenic monkeys overexpressing MeCP2. Nature 530, 98–102. [PubMed: 26808898]

Lombardo MV, et al. , 2009. Atypical neural self-representation in autism. Brain 133, 611–624. [PubMed: 20008375]

Lord C, et al. , 2020. Autism spectrum disorder. Nat. Rev. Dis. Primers 6, 5. [PubMed: 31949163]

Lu H, et al. , 2012. Rat brains also have a default mode network. Proc. Natl. Acad. Sci. U. S. A 109, 3979–3984. [PubMed: 22355129]

Lu H, et al. , 2016. Loss and gain of MeCP2 cause similar hippocampal circuit dysfunction that is rescued by deep brain stimulation in a Rett syndrome mouse model. Neuron 91, 739–747. [PubMed: 27499081]

Micheva KD, Beaulieu C, 1996. Quantitative aspects of synaptogenesis in the rat barrel field cortex with special reference to GABA circuitry. J. Comp. Neurol 373, 340–354. [PubMed: 8889932]

Morita T, et al. , 2012. Emotional responses associated with self-face processing in individuals with autism spectrum disorders: an fMRI study. Soc. Neurosci 7, 223–239. [PubMed: 21936743]

Mullaney BC, et al. , 2004. Developmental expression of methyl-CpG binding protein 2 is dynamically regulated in the rodent brain. Neuroscience 123, 939–949. [PubMed: 14751287]

Na ES, et al. , 2012. A mouse model for MECP2 duplication syndrome: MeCP2 overexpression impairs learning and memory and synaptic transmission. J. Neurosci 32, 3109. [PubMed: 22378884]

Nan X, et al. , 1997. MeCP2 is a transcriptional repressor with abundant binding sites in genomic chromatin. Cell 88, 471–481. [PubMed: 9038338]

Narayanan NS, Laubach M, 2006. Top-down control of motor cortex ensembles by dorsomedial prefrontal cortex. Neuron 52, 921–931. [PubMed: 17145511]

Padmanabhan A, et al. , 2017. The default mode network in autism. Biol. Psychiatry Cognit. Neurosci. Neuroimag 2, 476–486.

Pagani M, et al. , 2019. Deletion of autism risk gene Shank3 disrupts prefrontal connectivity. J. Neurosci 39, 5299–5310. [PubMed: 31061091]

Perruchoud D, et al. , 2014. Focal dystonia and the Sensory-Motor Integrative Loop for Enacting (SMILE). Front. Hum. Neurosci 8, 458. [PubMed: 24999327]

Qi S, et al. , 2018. Multimodal fusion with reference: searching for joint Neuromarkers of working memory deficits in schizophrenia. IEEE Trans. Med. Imaging 37, 93–105. [PubMed: 28708547]

Qiu Z, 2018. Deciphering MECP2-associated disorders: disrupted circuits and the hope for repair. Curr. Opin. Neurobiol 48, 30–36. [PubMed: 28961504]

Ramocki MB, et al. , 2010. Autism and other neuropsychiatric symptoms are prevalent in individuals with MeCP2 duplication syndrome. Ann. Neurol 66, 771–782.

Rane P, et al. , 2015. Connectivity in autism: a review of MRI connectivity studies. Harv. Rev. Psychiatry 23, 223–244. [PubMed: 26146755]

Semple BD, et al. , 2013. Brain development in rodents and humans: identifying benchmarks of maturation and vulnerability to injury across species. Prog. Neurobiol 106–107, 1–16.

Sengupta P, 2013. The laboratory rat: relating its age with human's. Int. J. Prev. Med 4, 624–630. [PubMed: 23930179]

Shoji H, Miyakawa T, 2019. Age-related behavioral changes from young to old age in male mice of a C57BL/6J strain maintained under a genetic stability program, 39, pp. 100–118.

Silverman JL, et al. , 2010. Behavioural phenotyping assays for mouse models of autism. Nat. Rev. Neurosci 11, 490–502. [PubMed: 20559336]

Smith Y, et al. , 2004. The thalamostriatal system: a highly specific network of the basal ganglia circuitry. Trends Neurosci 27, 520–527. [PubMed: 15331233]

Sui J, et al. , 2018. Multimodal neuromarkers in schizophrenia via cognition-guided MRI fusion. Nat. Commun 9, 3028. [PubMed: 30072715]

Sui J, et al. , 2020. Neuroimaging-based individualized prediction of cognition and behavior for mental disorders and health: methods and promises. Biol. Psychiatry 88, 818–828. [PubMed: 32336400]

Sumiyoshi A, et al. , 2014. Regional gray matter volume increases following 7days of voluntary wheel running exercise: a longitudinal VBM study in rats. NeuroImage 98, 82–90. [PubMed: 24816532]

Sumiyoshi A, et al. , 2019. Physiological considerations of functional magnetic resonance imaging in animal models. Biol. Psychiatry Cognit. Neurosci. Neuroimag 4, 522–532.

Tavassoli T, et al. , 2018. Sensory reactivity, empathizing and systemizing in autism spectrum conditions and sensory processing disorder. Dev. Cogn. Neurosci 29, 72–77. [PubMed: 28579480]

Torre E, et al., 2016. Synchronous spike patterns in macaque motor cortex during an instructed-delay reach-to-grasp task, 36, pp. 8329–8340.

Van Esch H, et al. , 2005. Duplication of the MECP2 region is a frequent cause of severe mental retardation and progressive neurological symptoms in males. Am. J. Hum. Genet 77, 442–453. [PubMed: 16080119]

Vann SD, et al. , 2009. What does the retrosplenial cortex do? Nat. Rev. Neurosci 10, 792–802. [PubMed: 19812579]

Varghese M, et al. , 2017. Autism spectrum disorder: neuropathology and animal models. Acta Neuropathol 134, 537–566. [PubMed: 28584888]

Vesuna S, et al. , 2020. Deep posteromedial cortical rhythm in dissociation. Nature 586, 87–94. [PubMed: 32939091]

Yu B, et al. , 2020. Reversal of social recognition deficit in adult mice with MECP2 duplication via normalization of MeCP2 in the medial prefrontal cortex. Neurosci. Bull 36, 570–584. [PubMed: 32144612]

Zhan Y, et al. , 2020. Diagnostic classification for human autism and obsessive-compulsive disorder based on machine learning from a primate genetic model. Am. J. Psychiatry 178, 65–76. [PubMed: 32539526]

Zhang Z-W, et al., 2010. MeCP2 Is Required for Normal Development of GABAergic Circuits in the Thalamus, 103, pp. 2470–2481.

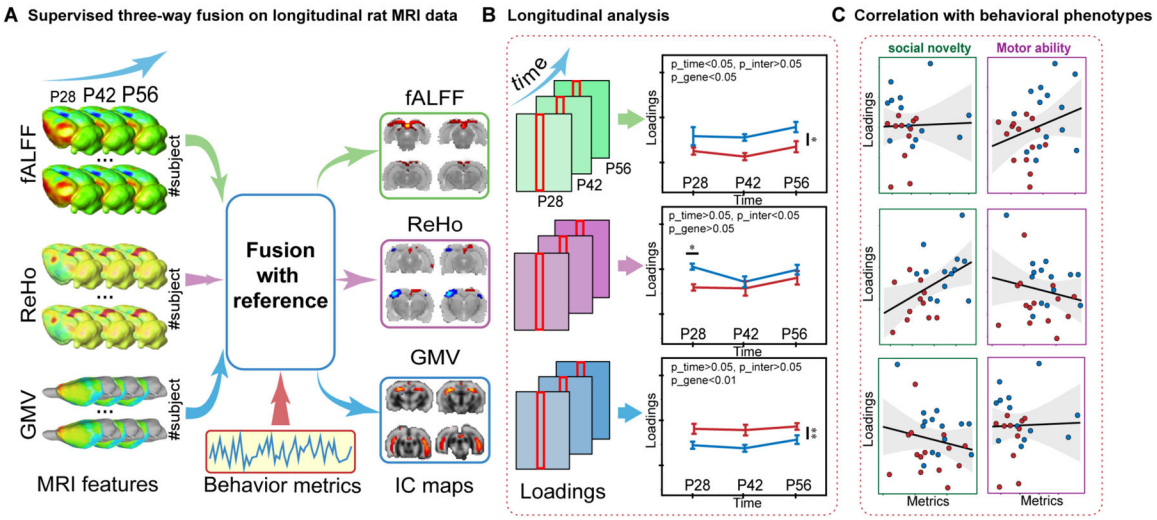

Fig. 1. Flowchart of the whole analysis.

(A) To identify behavior-related multimodal network and illustrate their developmental trajectories, we performed reference-guided multimodal fusion using MCCAR + jICA on rats at postnatal 28 days old (P28), 42 days old (P42) and 56 days old (P56). Three MRI features were jointly decomposed and supervised by different behavioral metrics, *i.e.*, motor ability score and social novelty time. **(B)** After fusion, a linear mixed-effect model was employed on the loadings of the derived components to test the group difference and time-varying effect spanning three developmental milestones. **(C)** Correlation coefficients with metrics of sociability and motor ability were calculated.

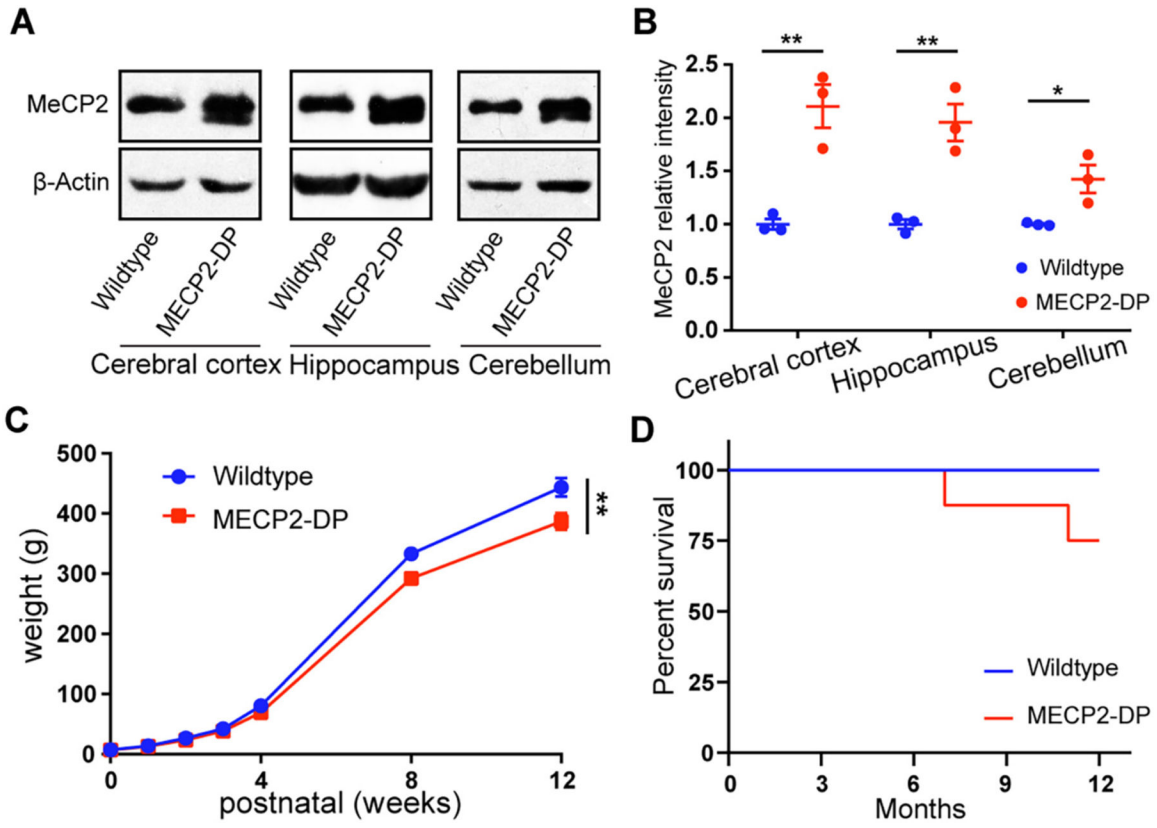

Fig. 2. Physiological features of MECP2-DP rats.

(**A-B**) Western blot analysis of brain tissues obtained from MECP2-DP rats and wildtype rats. (**C**) Longitudinal analysis of body weights. (**D**) Recordings of survival rate (MECP2-DP: MECP2 duplication; * $p < 0.05$; ** $p < 0.01$; *** $p < 0.001$).

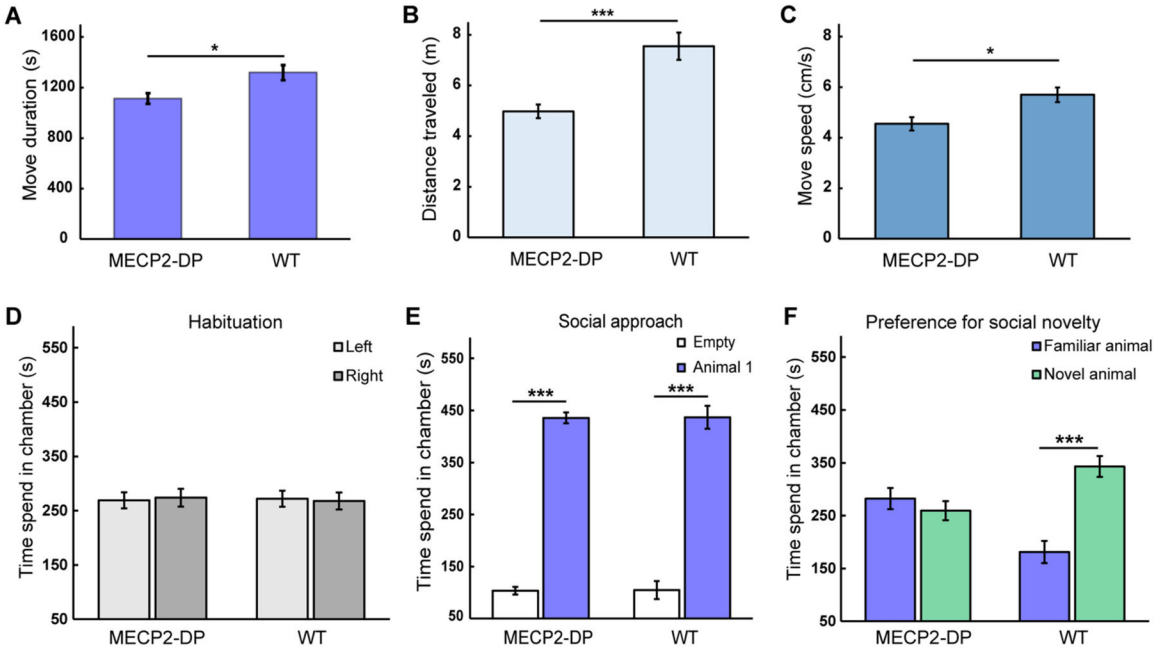

Fig. 3. Behavioral phenotypes of MECP2-DP rats.

(**A-C**) Results of the open-field test. The locomotor duration, distance and speed of MECP2-DP rats were significantly decreased compared with those of normal rats. (**D-F**) Results of the three-chamber test. (**D**) In the habituation session, the residence time differences on the left side and right side were not significant. (**E**) After introducing a male intruder, both groups spent more time with companions. (**F**) After introducing a new male intruder, unlike WT rats, the MECP2-DP rats did not show significant preferences over the novel animal. (MECP2-DP: MECP2 duplication; WT: wildtype; * $p < 0.05$; ** $p < 0.01$; *** $p < 0.001$).

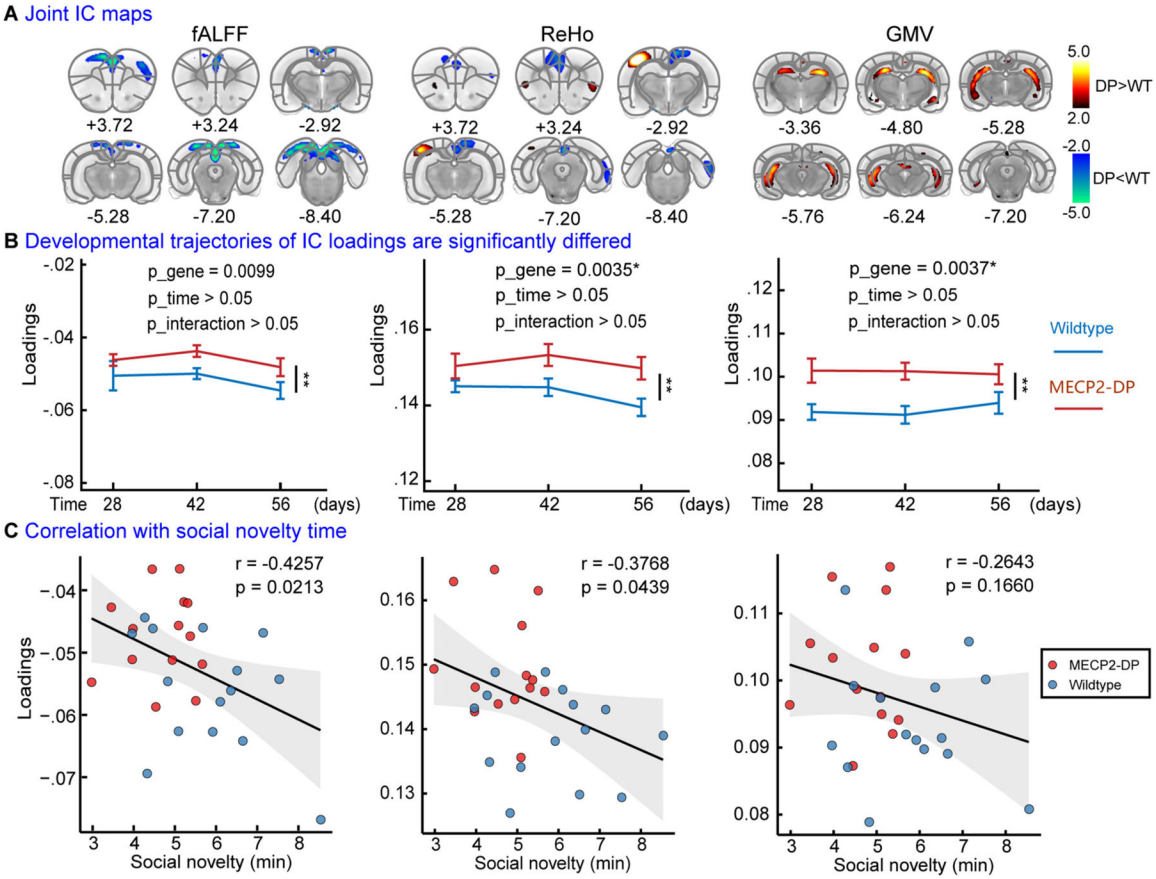

Fig. 4. Multimodal MRI patterns underlying social deficits in MECP2-DP rats.

(**A**) The identified fALFF-ReHo-GMV multimodal independent components (ICs) underlying social deficits mainly encompassed regions of the dorsal medial prefrontal cortex, retrosplenial cortex, motor cortex, visual cortex and hippocampus. The spatial map of each single modality IC was transformed to Z scores and visualized at $|Z| > 2$. The color map marked the contribution of voxels to the loadings of the IC. (**B**) The developmental trajectories of the identified covarying patterns are shown as changes of loadings along the three developmental milestones. The developmental trajectories of the fALFF, ReHo and GMV patterns in MECP2-DP rats were significantly differed from that in wildtype rats (gene effect: * $p < 0.05$; ** $p < 0.01$), whereas changes of the three patterns along the developmental milestones were not significantly differed (time effect and interaction effect of genotype-by-time were not significant). (**C**) Correlations between social novelty time and loadings of the identified multimodal components at postnatal 56 days old. Social novelty time was negatively correlated with loadings of the fALFF component and the ReHo component.

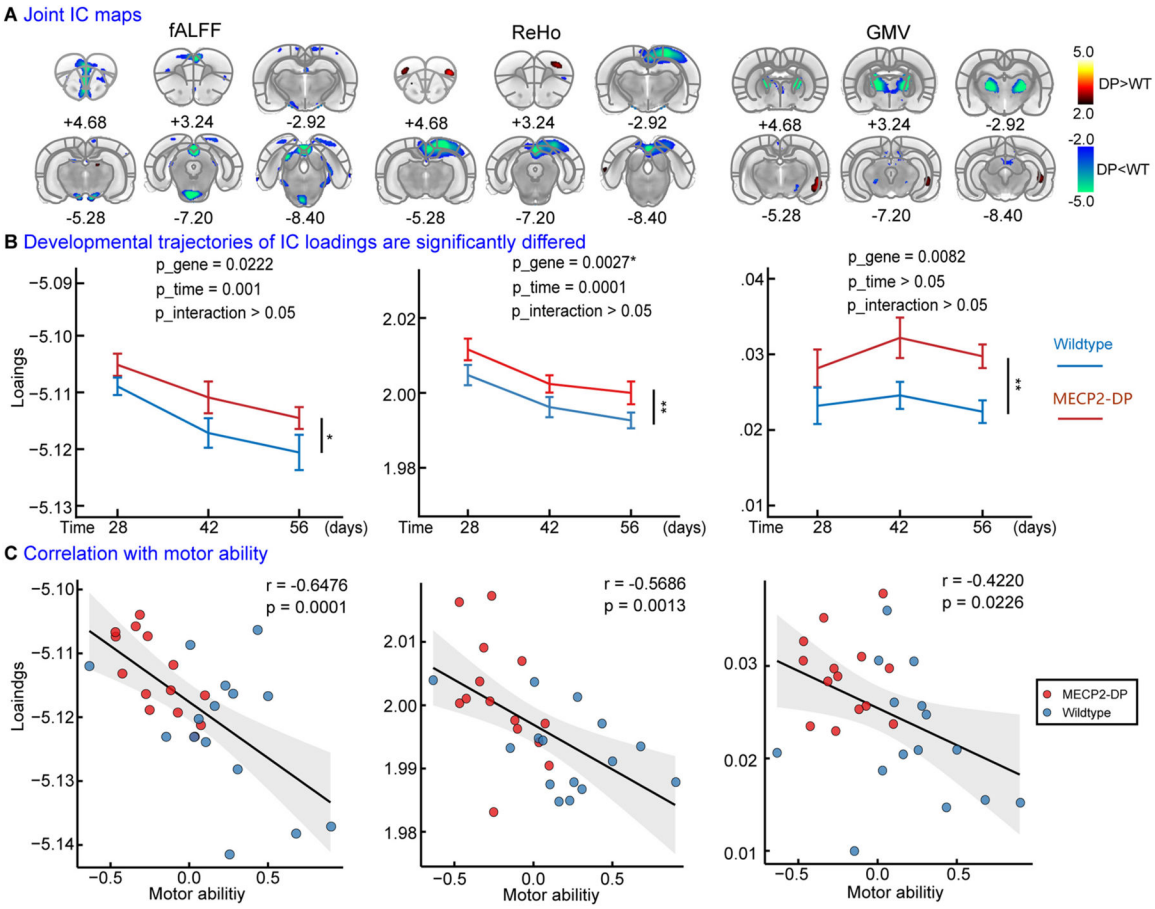

Fig. 5. Multimodal MRI patterns underlying motor deficits in MECP2-DP rats.

(**A**) The identified fALFF-ReHo-GMV multimodal independent components (ICs) underlying motor deficits mainly encompassed regions of the dorsal medial prefrontal cortex, retrosplenial cortex, motor cortex, somatosensory cortex, visual cortex, pontine nuclei, pineal gland and thalamus. The spatial map of each single modality IC was transformed to Z scores and visualized at $|Z| > 2$. The color map marked the contribution of voxels to the loadings of the IC. (**B**) The developmental trajectories of the identified brain network are shown as changes of loadings along the three developmental milestones. The developmental trajectories of the fALFF, ReHo and GMV patterns in MECP2-DP rats were significantly differed from that in wildtype rats (gene effect: * $p < 0.05$; ** $p < 0.01$). Loadings of the fALFF and ReHo patterns were significantly decreased along the developmental milestones, *i.e.*, the fALFF and ReHo of involved regions were increased along the development (time effects were significant). (**C**) Correlations between motor ability scores and loadings of the identified multimodal components at postnatal 56 days. Motor ability scores were negatively correlated with the loadings of the three components.

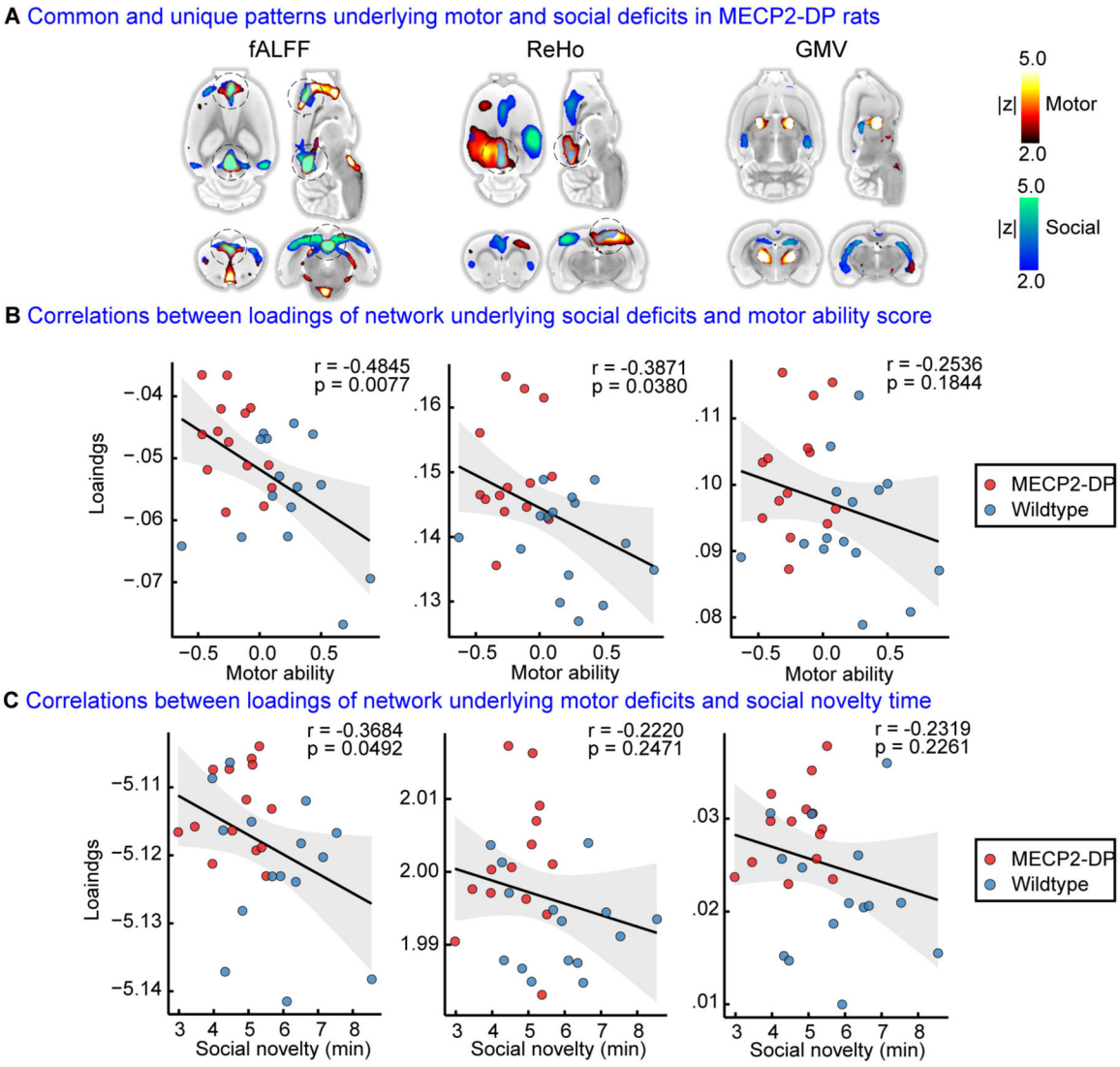

Fig. 6. Converged functional alterations underlying behavioral deficits in MECP2-DP rats.

(**A**) The *Z*-scored spatial maps of multimodal brain networks underlying motor deficits and social deficits were overlapped. The red regions marked the network associated with motor ability, and the blue regions marked the network associated with social ability. The brightness showed the absolute value of *Z* scores, *i.e.*, the contributions of the voxels to the group-level loadings. The black dash circles marked the primary overlapped regions, involving the dorsal medial prefrontal cortex, retrosplenial cortex. **(B)** Correlations between loadings of the multimodal networks underlying social deficits and motor ability scores. Loadings of the fALFF network and the ReHo network negatively correlated with motor ability score. **(C)** Correlations between the loadings of the multimodal networks underlying motor deficits and social novelty time. Loadings of the fALFF network negatively correlated with motor ability scores. (For interpretation of the references to color in this figure legend, the reader is referred to the web version of this article.)